Transport Models for Swelling and Dissolution of Thin Polymer Films

J. S. PAPANU,* D. S. SOANE (SOONG), A. T. BELL, and D. W. HESS, *Department of Chemical Engineering, University of California, Berkeley, California 94720*

Synopsis

Fundamental models have been developed to describe swelling and dissolution of glassy polymer thin films. The models account for solvent penetration by either Fickian or Case II diffusion mechanisms. The convective flux due to local swelling as the solvent penetrates is included. Chain disentanglement at the polymer-developer solution interface is scaled with the local solvent concentration and polymer molecular weight using reptation theory. The effective surface concentration during dissolution is estimated by applying thermodynamics of swollen networks to the entangled polymer. Swelling and dissolution of thin polymer films have direct application to microlithography. Various molecular and processing parameters affect the outcome of resist development. The utility of the models for selecting appropriate developer solvents, minimizing resist swelling, and providing a better understanding of the swelling and dissolution of resists is demonstrated.

INTRODUCTION

Thin polymer films are used for lithographic image transfer during the fabrication of microelectronic devices. After irradiation in selected areas, resist films are immersed in a solvent to develop the image. Often the maximum circuit density is dictated by the resolution limits of lithography, and these limits depend critically on the development step. If swelling is appreciable, then features will be distorted, and if dissolution is too rapid to control easily, undercutting due to overdevelopment will result. Thus, swelling and dissolution rate must be tightly controlled.

Swelling results from the penetration of solvent into the polymer. Solvent penetration involves diffusion of solvent molecules through the polymer matrix and local relaxation of polymer segments. The relative rates of relaxation and diffusion can be described by a diffusional Deborah number,[1,2]

$$D_D = t_R/t_D \tag{1}$$

where t_R is a characteristic relaxation time of the polymer–solvent system and t_D is the characteristic diffusion time. For rapid relaxation rates, i.e., small D_D values, penetration is diffusion limited and normal Fickian transport is observed; this mode is common for penetration in rubbery polymers. Fickian diffusion is also observed for large values of D_D (> 10). At such high

*Current address: Philips Research Laboratories Sunnyvale, Signetics Corporation, Sunnyvale, CA 94088.

Journal of Applied Polymer Science, Vol. 38, 859–885 (1989)
 CCC 0021-8995/89/050859-27$04.00

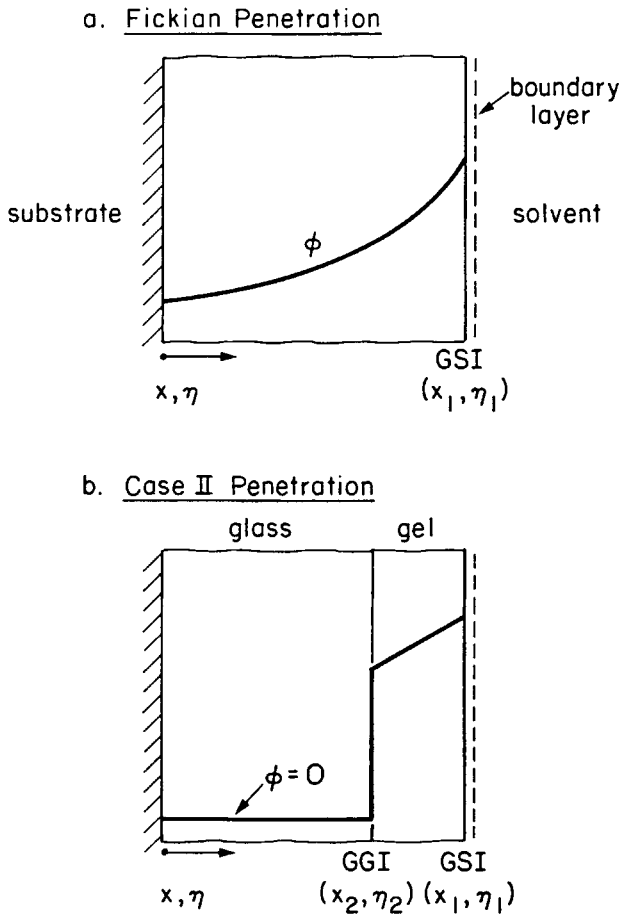

Fig. 1. Concentration profiles and boundary positions for (a) Fickian and (b) Case II penetration models. The gel–solvent interface (GSI) and gel–glass interface (GGI) are denoted by x_1 and x_2, respectively.

values of D_D, diffusion is relaxation limited, and the process is similar to diffusion in solids. A typical Fickian concentration profile in a polymer film is illustrated in Figure 1(a).

When relaxation times are comparable to diffusion times, non-Fickian behavior is observed. Sorption in glassy polymers is typically characterized by a sharp front (interface) between unpenetrated glass and swollen polymer that propagates into the film, initially at a constant rate. This situation is referred to as Case II diffusion.[3] The concentration profile for this case is depicted in Figure 1(b). For Case II diffusion, the profile trailing the sharp front is described by Fickian diffusion. Temperature and film thickness determine the transport mechanism. At lower temperatures, relaxation times are usually much longer than characteristic diffusion times, but at higher temperatures these times are similar (relaxation processes have higher activation energies). At temperatures where penetration is initially Case II, the film thickness determines whether apparent Fickian mass uptake will be observed. For thin

films, the diffusional resistance of the swollen gel is negligible, and relaxation at the gel/glass front will control the kinetics. In thicker films, the diffusional resistance of the swollen region becomes significant as the front moves inward, and Fickian diffusion of solvent between the polymer surface and the penetrating front eventually limits the swelling rate.[4]

Solvent penetration is the first step of polymer dissolution. The solvent enhances the mobility of polymer chains by converting the glassy matrix to a swollen, rubbery material. If the solvent and polymer have dissimilar solubility parameters (i.e., they are thermodynamically incompatible), then only swelling will be observed. However, if the solubility parameters are similar, polymer chains at the polymer–solvent interface will disentangle from the swollen matrix. Several limiting cases of dissolution can be envisioned, depending on the relative kinetics of solvent penetration, chain disentanglement, and external mass transfer. If external mass transfer is assumed to be rapid, the degree of swelling during dissolution depends on the relative rates of penetration and disentanglement. When penetration is rapid relative to disentanglement, an appreciable swollen surface layer forms, whereas minimal surface swelling is observed when the chains rapidly disentangle as the solvent permeates.

Models that describe swelling and dissolution of polymers have been reported for both general applications and resist processing in particular. Fickian swelling of polymers[5] has been modeled with standard Fickian diffusion models.[6] These models do not account for thickness changes due to swelling as the solvent penetrates. Thickness changes can be included, however, if the spatial coordinate, concentration, and diffusivity are defined such that the frame of reference is fixed with respect to a constant amount of polymer.[7]

Several models have been proposed to describe Case II penetration in the absence of dissolution. Some of these approaches use a diffusivity which is a function of stress or time,[8,9] or which is a stepwise function of concentration.[9] Two significantly different approaches to Case II diffusion have also been reported. One[10] is based on the viscous response of the polymer to the osmotic pressure developed by the presence of the penetrating solvent. Activity profiles and strain of the polymer due to the viscous response are solved simultaneously. The second model[11] is based on the phenomenological similarity of penetration with crazing (stress-induced formation of microcracks). The penetration of the sharp front is described by a kinetic expression which is proportional to the difference between the stress level at the front and the critical stress for crazing. The Fickian diffusion equation is solved in the penetrated region, thereby determining the solvent concentration profile behind the front. In its initial version, this model did not account for local swelling, so that penetration of the front and Fickian diffusion in the swollen region occurred without changing the film thickness. However, the model has been updated to include local swelling and polymer thickness changes.[12] Early dissolution models were semiempirical fits to dissolution rate data. For instance, the effects of molecular weight and temperature on the dissolution rate of polystyrene pellets in toluene were found to obey the relation[13]

$$R = R_0 \frac{\exp(-E_a/kT)}{M^A} \tag{2}$$

where R is the dissolution rate, M is the molecular weight, R_0 is a constant, E_a is the activation energy for dissolution, A is a constant (~ 0.5), T is temperature, and k is Boltzmann's constant. This equation fit the data reasonably well over the molecular weight range 10^3–10^5 g/mol. The decrease in dissolution rate with molecular weight of the polymer was attributed to entanglement effects. Later studies[14] with exposed and unexposed PMMA resists (~ 1000 nm thick) in ketone/alcohol developers showed that dissolution rate correlated well with an expression similar to eq. (2),

$$R = \left(B + R_0/M_f^{\alpha}\right)\exp(-E_a/kT) \tag{3}$$

where B is the high molecular weight limit rate constant, M_f is the fragmented molecular weight, and α is a model constant. The fragmented molecular weight accounts for chain scissioning induced by e-beam exposure.

A fundamental model for resist dissolution with Fickian penetration has been reported.[15] The model accounts for thickness increase due to local swelling and also thickness loss due to chain disentanglement at the surface of the film. Attempts to extend the model to pseudo Case II penetration by using diffusivity constitutive equations with nearly discontinuous concentration dependencies led to computational difficulties.

The work reviewed to this point has been applicable to single component resists. Several models for positive photoresist development have also been published.[16–19] Positive photoresists consist of two components, a base resin and a photoactive component, which also serves as a solubility inhibitor. Upon exposure, the inhibitor is altered, increasing the dissolution rate of the exposed regions in the developing solution. The positive resist models use empirical relations between the dissolution rate and local inhibitor concentration.

The objective of our work was to develop fundamental models for predicting the swelling and dissolution of thin polymer films (~ 1000 nm). This paper discusses the formulation of the models and presents a number of simulations to illustrate the influence of selected parameters. We also demonstrate how the models can be used to guide the selection of processing conditions to achieve high quality lithographic images. The application of the transport models to interpret experimental swelling and dissolution data will be presented in companion articles.[20,21]

THEORETICAL DEVELOPMENT

Two separate swelling/dissolution models are developed in this section—one for Fickian diffusion and one for Case II transport. Two models are necessary to span both penetration regimes. Penetration equations are discussed first, and then disentanglement kinetics are described. Our Fickian model closely follows the Fickian dissolution model discussed above,[15] and our Case II model is based on the stress driven penetration model.[11] The stress-driven approach was selected over the viscous response model since it accounts for residual stresses and differential swelling stresses, terms which could be significant for thin spun-on films. The primary contributions of the present work are the extension of the Case II model to include dissolution, the

development of a fundamental expression for the disentanglement rate, and the estimation of the effective surface composition during dissolution.

Fickian Penetration

The Fickian model is most appropriate for rubbery polymers, and is also needed for the swollen region in the Case II model. The model is one-dimensional and has one moving boundary [Fig. 1(a)], the gel–solvent interface (GSI), where the penetrated polymer is referred to as a "gel." For a fixed frame of reference with respect to the laboratory, the local mass flux of solvent in the polymer, j_s, is given by

$$j_s = -D_s(C_s)\frac{\partial C_s}{\partial x} \tag{4}$$

where D_s is diffusivity and C_s is the solvent mass concentration. Now

$$C_s = w_s\rho \tag{5}$$

where w_s is the mass fraction of solvent and ρ is the density of the mixture. If ideal mixing is assumed,

$$\rho = \sum_i \phi_i\rho_i \tag{6}$$

where ϕ_i and ρ_i are the volume fraction and density, respectively, of component i. For solvent (1)/polymer (2) binary mixtures,

$$C_s = (\rho_1 V_1)\frac{(\phi_1\rho_1 + \phi_2\rho_2)}{(\rho_1 V_1 + \rho_2 V_2)} = (\rho_1\phi_1)\frac{(\phi_1\rho_1 + \phi_2\rho_2)}{(\rho_1\phi_1 + \rho_2\phi_2)} = \rho_1\phi_1 \tag{7}$$

Here V_i is the volume of component i in some control volume. Thus j_s can be written

$$j_s = -D_s(\phi_1)\rho_1\frac{\partial\phi_1}{\partial x} \tag{8}$$

A "flux" or diffusive velocity can then be expressed as (dropping subscripts on ϕ and D),

$$j_s' = -D(\phi)\frac{\partial\phi}{\partial x} \tag{9}$$

where j_s' equals j_s/ρ_1. Since the solvent and polymer are assumed to be incompressible and to mix with no volume change, the local swelling velocity v is given by

$$v = -j_s' = D(\phi)\frac{\partial\phi}{\partial x} \tag{10}$$

This velocity corresponds to that of the polymer matrix (or "network") as it expands in the positive η direction.

Relative to a stationary observer, the conservation equation for solvent in the polymer film is expressed as

$$\frac{\partial \phi}{\partial t} = -\frac{\partial (j_s' + \phi v)}{\partial x} = -\frac{\partial [-D(\phi)\partial \phi/\partial x + \phi D(\phi)\partial \phi/\partial x]}{\partial x} \tag{11}$$

An assumption inherent in this equation is that imbibed solvent is carried along with the swelling polymer matrix. Expanding the right-hand side of eq. (11) and expressing the diffusivity as $D = D_0 f(\phi)$ (where D_0 is a front factor that depends on temperature) gives

$$\frac{\partial \phi}{\partial t} = (1 - \phi)D_0 f(\phi)\frac{\partial^2 \phi}{\partial x^2} + \left(\frac{\partial \phi}{\partial x}\right)^2 \left[(1 - \phi)D_0 \frac{df}{d\phi} - D_0 f(\phi)\right] \tag{12}$$

This equation can be made dimensionless by introducing the variables,

$$\tau = D_0 t/L^2, \qquad \eta = x/L$$

where L is the initial film thickness. Substituting the dimensionless quantities yields

$$\frac{\partial \phi}{\partial \tau} = (1 - \phi)f(\phi)\frac{\partial^2 \phi}{\partial \eta^2} + \left(\frac{\partial \phi}{\partial \eta}\right)^2 \left[(1 - \phi)\frac{df}{d\phi} - f(\phi)\right] \tag{13}$$

The initial condition is solvent-free polymer except at the surface, where the immersed sample immediately reaches a fixed surface concentration,

$$\phi(\eta, 0) = 0, \qquad 0 < \eta < 1 \tag{14a}$$

$$\phi(\eta = 1, 0) = \phi^* \tag{14b}$$

This fixed surface concentration is also the boundary condition at the GSI, $\eta = \eta_1$ [Fig. 1(a)],

$$\phi(\eta_1, \tau) = \phi^* \tag{15}$$

For pure swelling, ϕ^* is set to the equilibrium solvent fraction. The equilibrium approach is not applicable for dissolution, since at equilibrium only one phase is present. An effective surface concentration must be used for dissolution, as will be discussed later. The second boundary condition is zero flux at the substrate interface,

$$\left.\frac{\partial \phi}{\partial \eta}\right|_{\eta=0} = 0 \tag{16}$$

Movement of the polymer–solvent interface in the absence of dissolution is

given by

$$\frac{d\eta_1}{d\tau} = -\left(\frac{L}{D_0}\right) j_s' \Big|_{\eta_1} = \left(\frac{L}{D_0}\right) v \Big|_{\eta_1} \tag{17}$$

The GSI position can be checked for consistency by performing a mass balance on the solvent.

Case II Penetration

As with the Fickian model, the Case II model is also one-dimensional, but now two moving boundaries must be followed, the gel–glass interface (GGI) and the GSI [Fig. 1(b)]. The kinetics of the penetrating front, $x = x_2$, are governed by the stress level according to

$$\frac{dx_2}{dt} = v_2 = -K(\sigma - \sigma_c) \tag{18}$$

where v_2 is the penetration velocity, K is a front factor, σ is the total stress, and σ_c is the critical stress for crazing. The parameters K and σ_c are assumed to be a functions of the particular polymer and temperature. The parameter K follows an Arrhenius temperature dependence, $K \sim \exp(-E_a/RT)$, where T is the absolute temperature, E_a is the apparent activation energy, and R is the gas constant. The critical stress is a linear function of temperature, $\sigma_c = \gamma(T_g - T)$, where γ is a constant, and T_g is the glass transition temperature of the polymer.

Total stress is comprised of several terms,

$$\sigma = \alpha\left(\pi_{\text{eq}} + \pi^E\right) + \sigma_{\text{ds}} \tag{19}$$

where α is a fit parameter that varies with temperature, π_{eq} is the equilibrium osmotic stress, π^E is the excess stress, and σ_{ds} is the differential swelling stress. The parameter α can be thought of as an amplification factor, since typically $\sigma_c > \pi$. It also accounts for the dependence of the front velocity on the local solvent concentration. The osmotic stress is given by Flory–Huggins theory,[22]

$$\pi_{\text{eq}} = \frac{RT}{V_1}\left[\phi - \chi\phi^2 - \frac{1}{X}\ln(1-\phi)\right] \tag{20}$$

where V_1 is the molar volume of the solvent, χ is the Flory–Huggins interaction parameter, and X is the ratio of molar volumes [$X = V_2/V_1$]. The solvent fraction in eq. (20) is that at the GGI. Excess stress is a nonequilibrium condition resulting from incomplete annealing and/or rapid quenching. The differential swelling stress is due to the volume mismatch of swollen polymer on top of unswollen glassy polymer. The swollen layer pulls on the rigid glass (tension), and the glass in turn constrains the swollen gel (compression). Tension on the glassy layer can open up the polymer and facilitate solvent penetration. Differential swelling stress is a function of the degree of swelling, the relaxation time of the swollen polymer, and the glass thickness.

To a first approximation only the osmotic pressure term need be considered, and this simplification is made in the work reported here. The excess stress contribution to σ should be minimal because resist films are annealed above T_g after spin coating. If one assumes that the film has significant lateral swelling, then order of magnitude estimates suggest that differential swelling stress is significant. However, our model assumes that the film swells perpendicular to the penetration direction, and this is supported experimentally.[20] For swelling in this direction, the differential swelling stress is not significant. Furthermore, swelling experiments[20] do not show an accelerating penetration rate as the glass thickness approaches zero, which would be expected if differential swelling stress is important (as the glass thickness decreases, deformation of the remaining glass must increase to balance the swelling stress).

In the gel layer behind the penetrating front, the Fickian diffusion equation [eq. (13)] is solved. The initial condition and the boundary condition at the GSI are identical to the Fickian model [eqs. (14) and (15)]. The boundary condition at the GGI differs, however. Here the convective flux due to penetration must be matched by the diffusive flux in the gel at the interface. That is, at $\eta = \eta_2$,

$$(1 - \phi) f(\phi) \frac{\partial \phi}{\partial \eta} = \frac{-L v_2 \phi}{D_0} \tag{21}$$

Also, while the diffusion equation is solved throughout the entire polymer for the Fickian case, it is solved only in the penetrated region of the polymer in the Case II situation. The movement of the GSI is given by eq. (18).

Case II penetration is characterized by a Peclet number (Pe),[11]

$$\text{Pe} = \frac{(\text{initial penetration velocity}) * (\text{initial thickness})}{(\text{diffusivity in the swollen region})} \tag{22}$$

If solvent diffusion in the swollen region is rapid relative to the penetration velocity (Pe $\ll$ 1), then the concentration profile in the swollen region will be quite flat, and the penetration velocity will be constant. If the diffusivity is low, or the film is relatively thick (Pe $\gg$ 1), the diffusional resistance of the swollen region will be significant. The concentration profile will no longer be flat, and the penetration velocity will decrease with time.

Dissolution

Surface Disentanglement

Once plasticized by a penetrant, polymer chains will disentangle if the solution thermodynamics are favorable. Reptation theory has been developed[23,24] to describe the dynamics of entangled polymer chains. This theory is applied here to predict how disentanglement rate scales with polymer molecular weight and concentration.

As a starting point, disentanglement rate (R_{dis}) is taken to be proportional to some characteristic length divided by a characteristic time. The monolayer thickness was chosen as the characteristic length, and the reptation time

constant (t_{rep}) was selected as the characteristic time. The monolayer thickness can be approximated by the radius of gyration (R_g) of the polymer molecule. Thus,

$$R_{dis} \sim R_g/t_{rep} \tag{23}$$

The reptation time constant is expected to be proportional to a characteristic length squared divided by a characteristic diffusivity. If the self-diffusion coefficient (D_{self}) is chosen as the characteristic diffusivity, the reptation time constant can be approximated as

$$t_{rep} \sim R_g^2/D_{self} \tag{24}$$

Combining eqs. (23) and (24) gives

$$R_{dis} \sim D_{self}/R_g \tag{25}$$

It has been shown in the literature[23,24] that

$$R_g \sim M^{0.5}/(1 - \phi)^{0.125} \tag{26}$$

and

$$D_{self} \sim 1/M^2(1 - \phi)^{1.75} \tag{27}$$

Thus, the disentanglement rate can be expressed as

$$R_{dis} = C/M^{2.5}(1 - \phi)^{1.625} \tag{28}$$

where C is an empirical constant.

Gel–Solvent Interface Movement

Equation (17), which describes movement of the GSI for Fickian and Case II penetration, must be modified to include dissolution. If external mass transfer is rapid, then the disentanglement and solvent penetration rates will determine the movement of this boundary:

$$\frac{d\eta_1}{d\tau} = \left.\frac{\partial \phi}{\partial \eta}\right|_{\eta_1} - \bar{R} \tag{29}$$

where $\bar{R}$ is the dimensionless dissolution velocity. This general expression can be used for pure swelling by setting the surface attrition term to zero.

If external mass transfer is slow relative to disentanglement, polymer chains will accumulate on the solvent side of the GSI. To be rigorous, the diffusion equation should be solved for dissolved polymer in the liquid phase.[15] Using the resulting profiles, the boundary movement can be determined from

$$\frac{d\eta_1}{d\tau} = \left[\left.\frac{\partial \phi}{\partial \eta}\right|_{\eta_1}\right]_{pp} + \left[\left.\frac{\partial(1 - \phi)}{\partial \eta}\right|_{\eta_1}\right]_{sp} \tag{30}$$

where pp and sp denote polymer and solvent phase, respectively. For facile external mass transfer, the sp term in eq. (30) is limited by R, and eq. (29) is appropriate. For our model, external mass transfer was approximated using mass transfer coefficients and the concentration difference between the interface ($\phi = \phi^*$) and the bulk solvent ($\phi = 0$). Naturally, there will always be a boundary layer or disentangled layer, but it will be negligible for high agitation rates or high polymer diffusivity. All cases presented in this paper assume rapid external mass transfer.

Effective Surface Concentration

In the models presented here, the concentration at the surface (GSI) is fixed as a boundary condition. The effective surface concentration during dissolution has not been treated fundamentally in the literature, and so a way to estimate this concentration was needed.

One approach for estimating the effective surface concentration is to calculate the shift in chemical potential of solvent in the swollen polymer due to the energetics of chain entanglements. As the solvent penetrates, the chains cannot disentangle instantaneously. There will be some resistance to penetration due to the elastic deformation of the entangled polymer. The theory presented below is based on the thermodynamics of a swollen network.[25] It includes the effects of MW, temperature, and solvent quality (interaction parameter), and treats temporary entanglements as if they were permanent crosslinks (the swollen network concept is used in the Case II viscous response model[10] to calculate activity profiles).

Elongation of the chains anchored at entanglements adds an extra term to the total free energy of the polymer/solvent mixture,

$$\Delta G_{\text{total}} = \Delta G_{\text{mixing}} + \Delta G_{\text{elastic}} \tag{31}$$

From Flory–Huggins theory,[22]

$$\Delta G_{\text{mixing}} = kT\left[n_1 \ln \phi_1 + n_2 \ln \phi_2 + \chi n_1 \phi_2\right] \tag{32}$$

where n_1 and n_2 are the number of solvent and polymer molecules, respectively. For elastic deformation,

$$\Delta G_{\text{elastic}} \sim -T\Delta S_{\text{elastic}} \tag{33}$$

and

$$\Delta S_{\text{elastic}} = -\frac{k\sigma_e}{2}\left[\alpha_x^2 + \alpha_y^2 + \alpha_z^2 - 3 - \ln(\alpha_x\alpha_y\alpha_z)\right] \tag{34}$$

where α_i is the extension ratio along the ith coordinate and $\sigma_e/2$ is the number of effective crosslinks. The transport models developed here are for one-dimensional penetration, and the thin polymer film is expected to swell primarily in the direction normal to the substrate. However, the polymer could swell laterally to some degree (and induce tensile stress on the glass at the GGI, as discussed earlier). Thus, both one- and three-dimensional cases

were considered. The one-dimensional approach will be described, and then the results for three-dimensional swelling will be presented. For one-dimensional swelling,

$$\alpha_s = V/V_0 = \alpha_z \tag{35a}$$

$$\alpha_x = \alpha_y = 1 \tag{35b}$$

where α_s is the swelling extension ratio, V_0 is the initial volume of unswollen polymer, and V is the volume of swollen polymer. Substituting eqs. (32)–(35b) into eq. (31) and differentiating ΔG_{total} with respect to moles of solvent gives the chemical potential difference between solvent in the polymer and pure solvent:

$$\mu_1 - \mu_1^0 = RT\left[\ln(1-\phi_2) + (1-1/X)\phi_2 + \chi\phi_2^2 + (V_1/V_0)(\sigma_e/2N)(2/\phi_2 - \phi_2)\right] \tag{36}$$

where ϕ_2 is the polymer volume fraction and $(\sigma_e/2N)$ is the number of moles of crosslinks.

Assume now that the number of moles of crosslinks can be replaced by the number of moles of entanglements. The number of entanglements per polymer molecule can be approximated by

$$\frac{\text{entanglements}}{\text{molecule}} = \frac{M}{M_e} - 1 \tag{37}$$

where M is the molecular weight of the chain and M_e is the molecular weight between entanglements. The number of moles of entanglements, N_e, is therefore

$$N_e = \frac{V_0\rho_2}{M}\left(\frac{M}{M_e} - 1\right) \tag{38}$$

From rheological studies,[26]

$$M_e \sim M_c/2 \tag{39}$$

where M_c is the critical molecular weight of the polymer. M_c is defined by a sharp increase in slope that is seen in a plot of viscosity vs. molecular weight, which is attributed to the onset of entanglements. It has also been shown[26] that, for concentrated solutions,

$$(M_e)_{\text{soln}}(1-\phi) = (M_e)_{\text{melt}} \tag{40}$$

and likewise for M_c. Since V_0 and ρ_2 apply to the unswollen polymer, $(M_e)_{\text{melt}}$ is more appropriate for estimating N_e. Substituting eqs. (38) and (39) into eq. (36) yields

$$\mu_1 - \mu_1^0 = RT\left[\ln(1-\phi_2) + (1-1/X)\phi_2 + \chi\phi_2^2 + V_1\rho_2(2/M_c - 1/M)(2/\phi_2 - \phi_2)\right] \tag{41}$$

A similar analysis for three-dimensional, unconstrained swelling, where $\alpha_s = \alpha_x = \alpha_y = \alpha_z$, yields

$$\mu_1 - \mu_1^0 = RT\left[\ln(1 - \phi_2) + (1 - 1/X)\phi_2 + \chi\phi_2^2 + V_1\rho_2(2/M_c - 1/M)\left(2\phi_2^{1/3} - \phi_2\right)\right] \quad (42)$$

Equation (42) is equivalent to eq. (41) except for the expansion term $(2/\phi_2 - \phi_2)$. Note that the molecular weight effect will be negligible at high MW for both one- and three-dimensional swelling. Also, the one-dimensional equation will have a much higher contribution of strain energy for high degrees of swelling, that is, as ϕ_2 approaches zero.

At equilibrium, the chemical potential of each component is equal in all phases. As an approximation, the equilibrium solvent composition in the polymer phase can be estimated by assuming that the solvent phase is pure. Thus, the left side of eq. (41) reduces to zero, and ϕ_2 can be calculated given χ. For pure swelling with no dissolution, ϕ_2 can be calculated similarly, except that the entanglement term in eq. (41) is also set to zero.

Values of ϕ_2 during dissolution can be determined from experiment if the assumption holds that the kinetic parameter a in the Case II model is independent solvent. If a is independent of solvent, values of a as a function temperature can be determined from swelling data. These values can then be applied to dissolution data to back out the effective surface concentration from the penetration rate. If the basic assumption that a is independent of solvent is not valid, then the surface concentration cannot be uniquely determined from penetration kinetics.

Solution Techniques

Transport models describing swelling and dissolution of polymer films are moving boundary problems, whose solutions have been recently reviewed.[27] In brief, location of the interface(s) is (are) part of the solution. The moving interface can be handled by either front-fixing or front-following techniques. In the former, variable transformations are used to fix the boundary location. This is most useful when no mass is lost from the system. With front-following methods, modified expressions for the derivative approximations are applied in the vicinity of the interface. Since the Case II model has two moving boundaries, and since mass is lost during dissolution, a front following method was developed for both the Fickian and Case II models.

A Crank–Nicolson implicit finite difference technique with a spatially fixed grid was used to solve the transport equations. An implicit technique was selected due to its greater stability and the high nonlinearity of the differential equations. Derivatives at the interface were approximated by implicit expressions that treat the boundary as a pseudo grid point. The expressions account for movement of the boundary between and across the fixed grid points in a manner similar to a Lagrangian interpolation formulation.[28]

In order to make the problem tractable, the conservation equation and boundary conditions were linearized by using values at the old time level. For

example, the conservation equation was linearized as

$$\left(\frac{\partial\phi}{\partial\tau}\right)_{s+1} = [(1-\phi)f(\phi)]_s\left(\frac{\partial^2\phi}{\partial\eta^2}\right)_{s+1} + \left(\frac{\partial\phi}{\partial\eta}\right)_s\left(\frac{\partial\phi}{\partial\eta}\right)_{s+1}\left[(1-\phi)\frac{df}{d\phi} - f(\phi)\right]_s \tag{43}$$

where the current time level for which a solution is to be obtained is denoted by an $s + 1$ subscript and the previous time level by s. Likewise, movement of the polymer–solvent boundary was linearized as

$$(\eta_1)_{s+1} = (\eta_1)_s + \Delta\tau\left(\frac{d\eta_1}{d\tau}\right)_s \tag{44}$$

and the boundary condition for the gel–glass interface in the Case II model was linearized as

$$\left[\left(\frac{\partial\phi}{\partial\eta}\right)\Big|_{\eta_2}\right]_{s+1} = \frac{-L(v_2)_s(\phi)_{s+1}}{D_0[(1-\phi)f(\phi)]_s} \tag{45}$$

Interface positions were calculated from velocities at the previous time level, and the diffusion equation was solved after the boundaries had been moved to their new positions. Additional details such as derivative approximations at the boundaries are given elsewhere.[29]

RESULTS AND DISCUSSION

Effective Surface Concentration

Before the Fickian and Case II models can be solved for either swelling or dissolution, the solvent volume fraction in the polymer at the GSI is needed [eq. (15)]. The equilibrium solvent fraction in the polymer as a function of χ at three molecular weights is shown in Figure 2(a) for pure swelling [eq. (41) with entanglement term omitted]. As expected, the equilibrium fraction in the polymer phase increases as χ decreases (better solvent or higher temperature), until eventually dissolution is reached ($\phi = 1.0$). Higher molecular weight requires a lower value of χ to reach dissolution, and yields a lower value of ϕ for a given value of χ. Note that except for low MW (20,000 g/mol), MW effects are negligible for typical nonsolvents ($\chi > 0.6$). Thus penetration rates of swelling agents are expected to be relatively independent of MW. Figure 2(b) shows the equilibrium solvent fraction for one-dimensional entanglement energetics [eq. (41)]. For values of $\chi > 0.9$, the predicted solvent fraction is comparable to that for no entanglements, but a downturn is seen at lower values of χ. The solvent quality is compensated by the increased strain energy at higher degrees of swelling. Molecular weight effects are insignificant at higher values of χ, but are observable at lower values of χ, although in the limit of high MW, the effects diminish even at low values of χ.

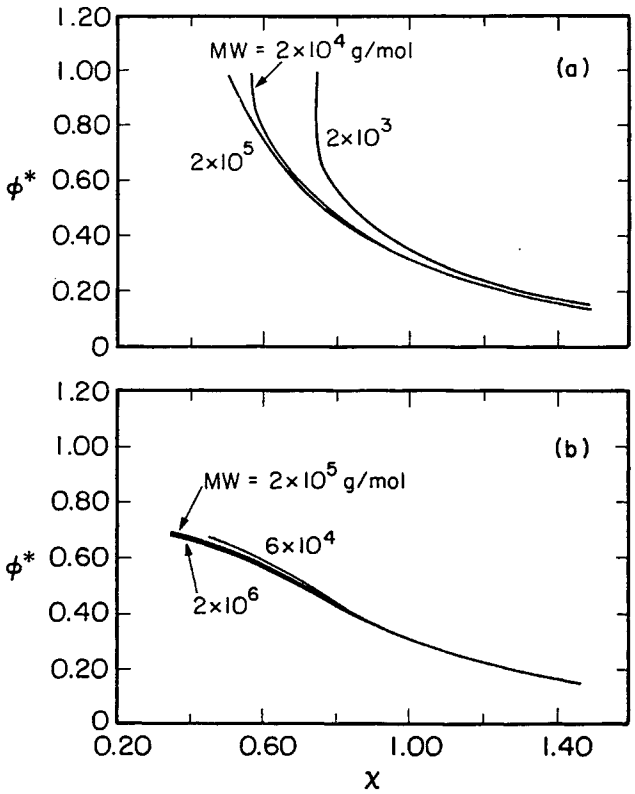

Fig. 2. Equilibrium solvent fraction in the polymer as a function of χ for (a) no entanglements and (b) one-dimensional swelling with entanglements.

Swelling and Dissolution

The characteristic parameter describing Fickian penetration is diffusivity. Several constitutive equations were used for the diffusivity. The concentration dependent factor was taken as unity, linearly dependent, or exponentially dependent on solvent volume fraction. An exponential dependence is consistent with experimental data for the diffusion of organic vapors in polymers,[30] and with the functional form for polymer solutions based on free volume concepts.[31] The exponential expression used was

$$f(\phi) = \exp[(\phi - \phi^*)/\beta] \tag{46}$$

where β is a constant.

Figure 3 shows movement of the polymer/solvent interface and the concentration profiles during Fickian swelling at several times for two concentration dependencies. In Figure 3(a) $f(\phi) = 1$, and in Figure 3(b) eq. (46) is used with $\beta = 0.5$. Other parameters are listed in the figure captions. Since D_0 is the same for both cases, the dimensionless times correspond to the same actual

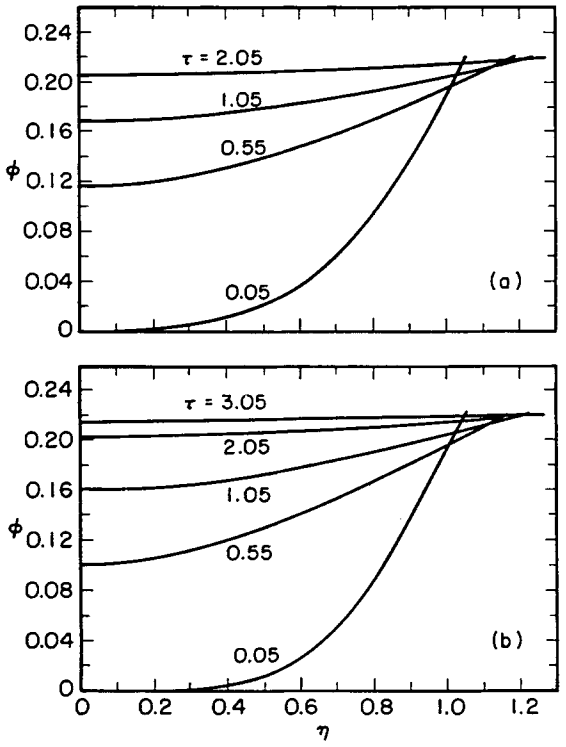

Fig. 3. Concentration profiles and boundary location for Fickian swelling at several dimensionless times for $D_0 = 5.0 \times 10^{-12}$ cm^2/s, $L = 10^{-4}$ cm, and $\phi^* = 0.22$: (a) concentration independent diffusivity; (b) exponential concentration dependence with $\beta = 0.5$.

times. A higher concentration dependence results in steeper concentration gradients and lower initial swelling rates.

Case II concentration profiles at several time levels for Pe = 0.001, i.e., rapid diffusion in the swollen layer, are shown in Figure 4. As expected, the concentration profile in the swollen region is flat, and the kinetics of the penetrating front controls the swelling. Figure 5 shows similar curves for Pe = 1, with the first three profiles corresponding to the same actual time levels as Figure 4 (dimensionless time is different since the diffusivity is lower). Some diffusional resistance in the swollen layer is observed, and this lowers the penetration rate since the concentration at the front is reduced.

The effect of decreasing χ at constant temperature, solvent molar volume, and Pe is seen by comparing Figures 6 and 4. For the better solvent, the surface fraction is higher and consequently so is the penetration rate. The penetration rate for $\chi = 0.88$ is 1.0×10^{-7} cm/s, whereas it is 1.3×10^{-6} cm/s for $\chi = 0.75$. Thus for $\tau = 440$ (440 s) the GGI is at $\eta = 0.54$ for the poorer solvent, and the GGI is at $\eta = 0.43$ for $\tau = 563$ (44 s) with the better solvent.

Figure 7 shows the positions of the GSI and GGI for dissolution of polymer with MW of (a) 200,000 g/mol and (b) 50,000 g/mol. The model parameters

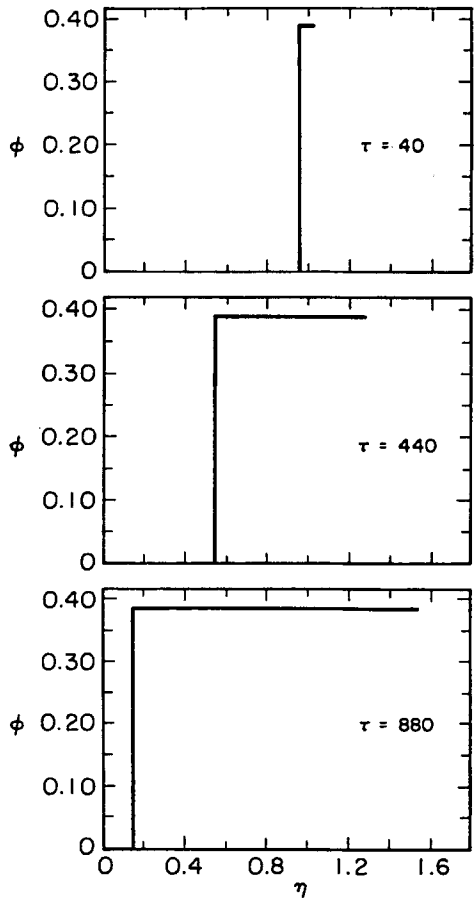

Fig. 4. Concentration profiles and boundary locations for Case II swelling at dimensionless times of (a) 40, (b) 440, and (c) 880. Concentration-independent diffusivity and $L = 10^{-4}$ cm, $a = 6.1$, $\chi = 0.876$, $K = 9.0 \times 10^{-9}$ cm/(s atm), $\sigma_c = 532$ atm, $V_1 = 76.5$ cm^3/mol, $D_0 = 10^{-8}$ cm^2/s, MW $= 2 \times 10^5$ g/mol, $T = 323$ K, and Pe = 0.001.

were selected such that this difference in MW would cause a switch from disentanglement to penetration control. Penetration was by a Case II mechanism with Pe = 0.001. The effective surface concentration was estimated using $\chi = 0.45$ in the one-dimensional entanglement equation [eq. (40)]. In Figure 7(a) the disentanglement rate is controlling due to the high MW. Rapid solvent penetration causes the film to swell completely before any appreciable dissolution occurs, and then the swollen film slowly dissolves. For the low MW situation [Fig. 7(b)], dissolution is penetration limited. Swelling is negligible and the two boundaries are essentially coincident. At intermediate molecular weights, dissolution with some swelling is expected.

Resist Processing

Having developed a model for the dissolution of thin polymer films, it is of interest to assess the utility of the model for selecting resist processing conditions. A desirable development process provides a moderate dissolution

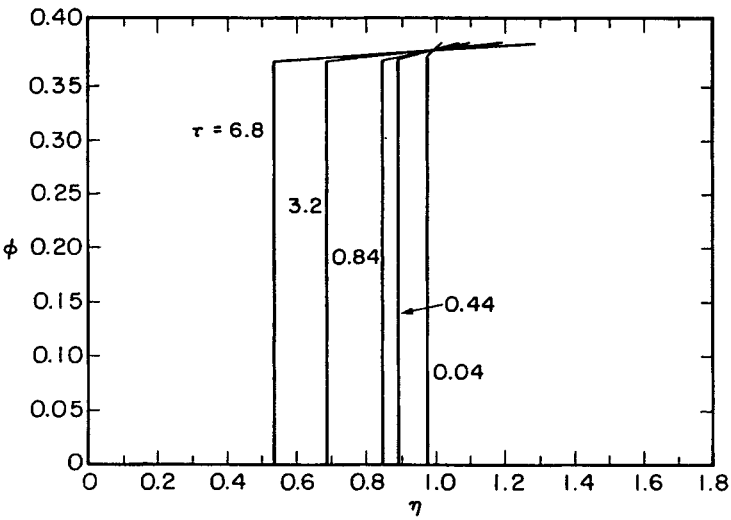

Fig. 5. Concentration profiles and boundary locations for Case II swelling at several dimensionless times. Parameters are the same as in Figure 4 except $D_0 = 1.0 \times 10^{-11}$ cm^2/s and Pe = 1.0. The first three profiles correspond to the same actual times as in Figure 4.

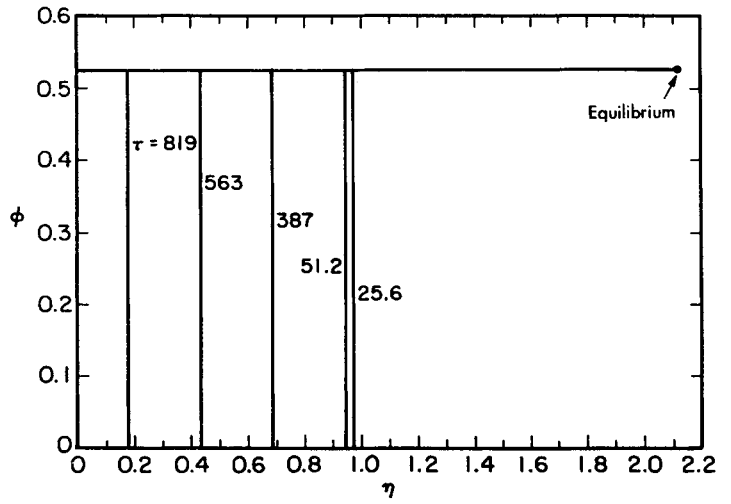

Fig. 6. Concentration profiles and boundary locations for Case II swelling at several dimensionless times. Parameters are $\chi = 0.75$, $\phi^* = 0.526$, and $D_0 = 1.3 \times 10^{-7}$ cm^2/s. All other parameters are the same as in Figure 4, including Pe = 0.001.

rate, minimal swelling, and high contrast or selectivity between exposed and unexposed polymer. A moderate dissolution rate allows process latitude in development time while maintaining a reasonable throughput. Typical development times are 20–100 s. Swelling will be minimized if dissolution is penetration limited. A high differential dissolution rate between exposed and unexposed resist ensures that removal and/or swelling of the desired regions will not be appreciable. To demonstrate how the models can be employed to

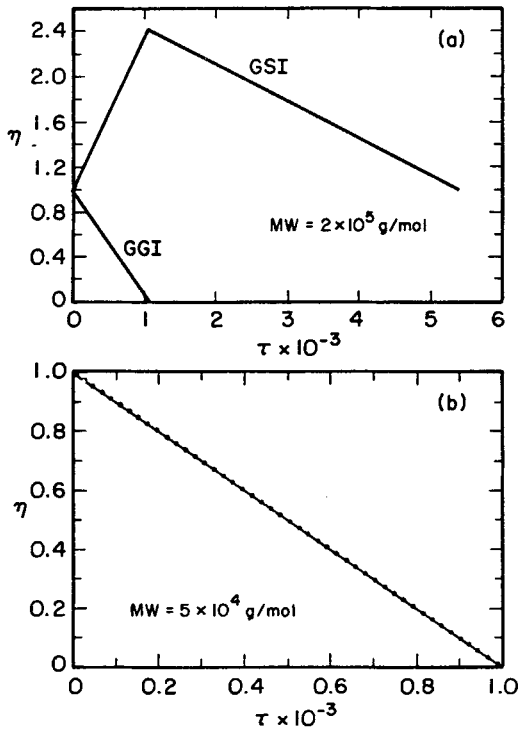

Fig. 7. GSI and GGI locations during dissolution as a function of dimensionless time for (a) MW = 200,000 g/mol, $\phi^* = 0.64$ and (b) MW = 50,000 g/mol, $\phi^* = 0.665$. Part (a) corresponds to disentanglement limited dissolution and part (b) corresponds to penetration limited dissolution. In (b), the location of the GSI is denoted by ●. Parameters for both cases are $L = 10^{-4}$ cm, $K = 9.0 \times 10^{-9}$ cm/(s atm), $a = 6.1$, $v = 0.45$, $T = 323$ K, $V_1 = 74.0$ cm^3/mol, $C = 5 \times 10^6$ cm(g/mol)$^{2.5}$/s, and $\sigma_c = 532$ atm.

help achieve these objectives, two hypothetical examples and a direct comparison with experimental data for PMMA dissolving in methyl isobutyl ketone will be presented. In the discussion below, the solvent penetration mechanism is assumed be Case II.

A moderate dissolution rate can be obtained via judicious selection of the developer. Consider a process where the temperature of the developer bath is fixed at 23°C, a typical operating condition. This implies that the thermodynamic quality of the developer can be changed only by varying the solvent. Assume that the disentanglement rate is rapid for the entire relevant molecular weight range, and ignore polydispersity effects. Finally, assume that exposed regions dissolve 10 times faster than unexposed polymer, which is a typical enhancement factor.[17,32] Then the solvent interaction parameter and molecular size, and to a small extent the polymer molecular weight, will determine the dissolution rate. In order to clear completely a 1000 nm film in 20–100 s, the dissolution (penetration) rate must be between 10 and 50 nm/s. Provided that valid a and K values have been obtained for the polymer of interest, the values of solvent molar volume and interaction parameter that give dissolution rates in the desired window can be mapped out.

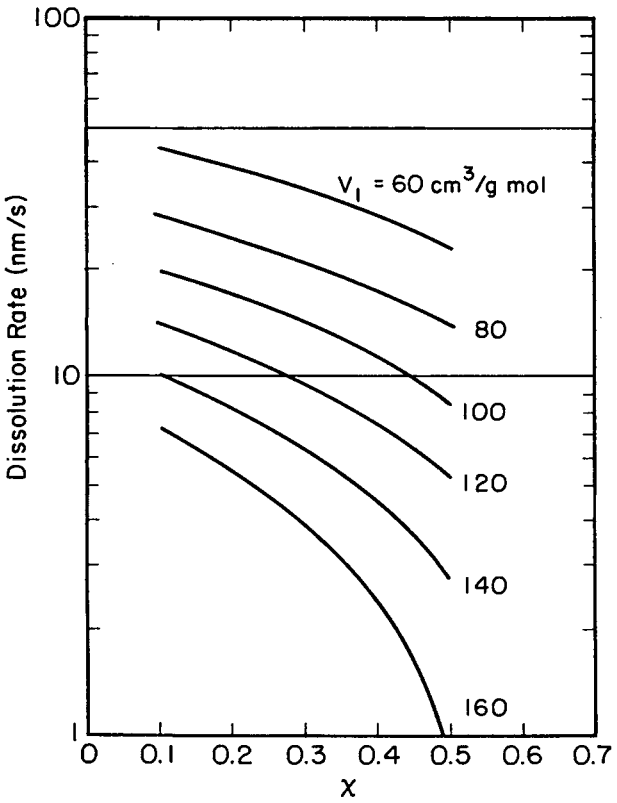

Fig. 8. Dissolution rate vs. χ for solvent molar volumes of 60–160 cm^3/(g mol). Dissolution is assumed to be penetration limited, and penetration occurs by Case II diffusion. Solid lines at 10 and 50 nm/s mark the lower and upper limits of the desired dissolution rate. Parameters are $T = 296$ K, $a = 8.0$, $K = 2.4 \times 10^{-10}$ cm/(s atm), $\sigma_c = 442$ atm, MW = 180,000 g/mol, and $M_c = 27{,}000$ g/mol. Rates are 10 times those for unexposed polymer.

Figure 8 shows dissolution rate (exposed regions) vs. χ ($0.1 < \chi < 0.50$) for several values of solvent molar volume. The value of K corresponds to that for poly(methyl methacrylate) (PMMA) an electron-beam resist, and was obtained from mechanical crazing[33] and solvent penetration data.[4] The value of a is an approximate value for the dissolution of PMMA in lower MW ketones. Swelling and dissolution data for PMMA[20,21] indicate that a varies with solvent, not just temperature. However, the values of a are relatively independent of solvent size except for very small molecules, and for a given solvent series an average value of a can be used. As can be seen in Figure 8, for solvent molar volumes of 140 and 160 cm^3/mol the dissolution rate is below the desired range. To be within the desired dissolution rate range for $V_1 =$ 120 cm^3/mol, χ must be < 0.27, and for $V_1 = 100$ cm^3/mol, χ must be < 0.45. As a practical example, consider PMMA in lower MW ketone developers, for which $\chi \sim 0.48$.[34] Methyl ethyl ketone ($V_1 = 90.0$ cm^3/mol) would give a desirable dissolution rate, but diethyl ketone ($V_1 = 106.1$ cm^3/mol) would dissolve the film too slowly.

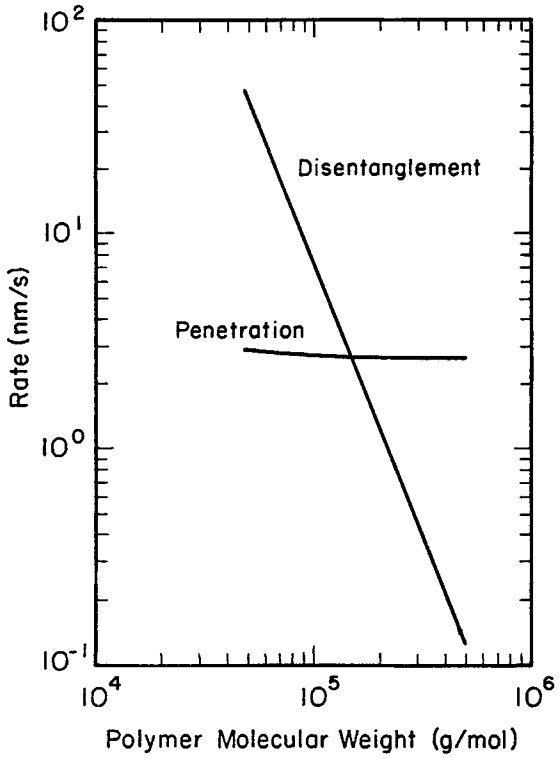

Fig. 9. Penetration and dissolution rates as a function of polymer molecular weight for the Case II dissolution model. The effective surface concentration is calculated using 1-D entanglement energetics. Model parameters are $T = 296$ K, $\chi = 0.45$, $K = 10^{-9}$ cm/(s atm), $V_1 = 90$ cm^3/mol, $\sigma_c = 450$ atm, and $C = 5 \times 10^5$ (g/mol)$^{2.5}$ cm/s.

Next consider the situation where increasing the polymer MW can shift the controlling mechanism from penetration to disentanglement. (The extremes of such a situation were depicted in Fig. 7.) Figure 9 shows penetration and disentanglement rates as a function of molecular weight. Typical values of the penetration parameters were used, and the value of the disentanglement rate factor, C [eq. (28)], was selected to give a switch in the controlling mechanism near 10^5 g/mol. Again note the relative insensitivity of penetration rate to molecular weight. At molecular weights < 150,000 g/mol, dissolution is penetration controlled, while at higher molecular weights dissolution is disentanglement controlled. As mentioned previously, to minimize swelling effects, dissolution should be penetration rate controlled. Consequently, for the parameter values selected, the molecular weight of the exposed region should not exceed 150,000 g/mol. If the constant C is adjusted, the disentanglement rate curve will be shifted up or down, and likewise changing solvent or temperature will shift the penetration rate curve. In either case, the intersection point will also shift. Hence, plots such as those in Figure 9 are useful for choosing molecular weights that ensure that dissolution will be penetration controlled.

The porosity of a resist increases during the exposure step.[32] Figure 9 can be used to demonstrate the influence of this porosity change on resist development. For example, consider a positive resist with an initial molecular weight

of 500,000 g/mol, and a post-exposure MW of 80,000 g/mol. Neglect polydispersity effects, and assume initially that porosity remains unchanged. Exposure increases the disentanglement rate by 2 orders of magnitude, which shifts the resist from a disentanglement controlled region to a penetration controlled region. Consequently, minimal swelling of the exposed resist is expected as it dissolves. The disentanglement rate of the unexposed resist is sufficiently low that only a small fraction will dissolve. However, the penetration rate in the exposed resist will be only slightly less than that in the exposed polymer. Thus, unexposed regions will swell appreciably, which could have detrimental effects on the developed image.

Now assume that porosity increases during exposure. Since the solvent molecules can more readily penetrate into the more porous film, the effective value of either K or σ_c is higher. Consequently, the penetration rate curve will shift upward for the exposed regions. If the penetration rate is substantially higher in the exposed regions, then the unexposed resist will not swell much in the time it takes to clear the image to the substrate. Thus, while the MW shift ensures minimal dissolution of the unexposed resist, increased porosity helps reduce the degree of swelling in unexposed resist.

The discussion on exposure effects has focused to this point on the kinetics of swelling and dissolution. The lowering of the average polymer MW by exposure can also affect the thermodynamics of dissolution. The MW shift could yield an exposed material which is soluble in the developer at the particular temperature, while the unexposed resist is insoluble. Then the relative dissolution rates of the exposed and unexposed regions are no longer a consideration. However, penetration kinetics will still determine the dissolution rate in the soluble regions and the degree of swelling in the insoluble portions of the resist.

Finally, the consistency of the model with experimental dissolution rates can be assessed. The dissolution rate vs. polymer MW for unexposed, monodisperse PMMA in methyl isobutyl ketone (MIBK) at 24.8°C[21,35] is shown in Figure 10. The dissolution rate scales approximately with 1/MW, and then levels off at high MW. Similar trends have been reported by other investigators.[14,36] *In situ* ellipsometric data[21] indicate that the dissolution of PMMA in MIBK is penetration controlled. (The dissolution rate is expected to decrease eventually at higher MW as disentanglement control is encountered.) Also shown in Figure 10 are penetration and disentanglement rate curves similar to those in Figure 9. The shift of the penetration rate curve in Figure 10 compared to Figure 9 is due to different values of the penetration parameters (see figure captions). For the penetration rate curve in Figure 10, the value of σ_c was obtained from mechanical crazing data for high MW, polydisperse PMMA,[37] and the parameter a was calculated from the average dissolution (penetration) rate of polydisperse, PMMA thin films in MIBK.[21] Since disentanglement control was not encountered experimentally, a value of C [eq. (28)] could not be determined. Thus, Figure 10 includes two disentanglement rate curves corresponding to possible values of C. Both values of C are sufficiently large that the dissolution rate is clearly controlled by the solvent penetration rate.

It is evident from Figure 10 that the penetration rate curve underestimates the dependence of dissolution (penetration) on molecular weight for MW up

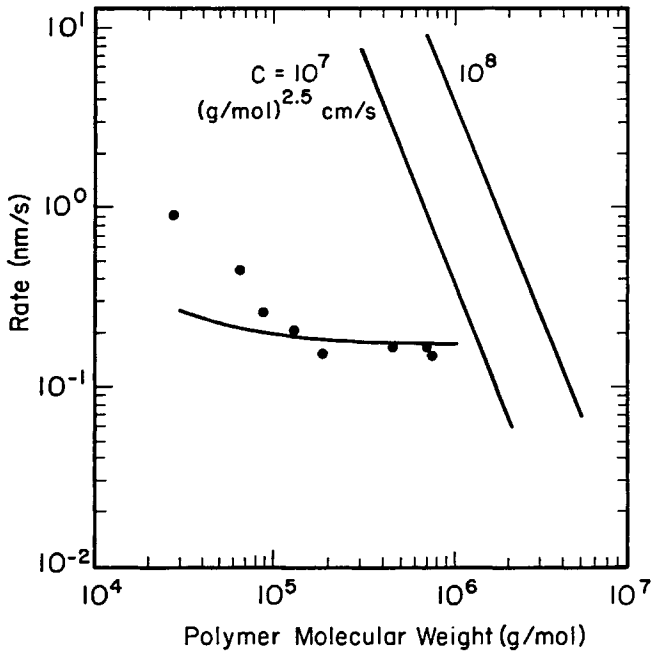

Fig. 10. Dissolution rate as a function of molecular weight for PMMA in MIBK at 24.8°C, and penetration and dissolution rate curves from the Case II model assuming 1-D entanglement energetics. Case II model parameters are $V_1 = 125.8$ cm^3/mol, $T = 297.9$ K, $a = 6.36$, $\chi = 0.4957$, $\sigma_c = 432$ atm, $K = 2.67 \times 10^{-10}$ cm/(s atm), and $C = 1.0 \times 10^7$ and 1.0×10^8 (g/mol)$^{2.5}$ cm/s.

to 1.5×10^5 g/mol (although it does fit the data quite well above this MW). The simplified (osmotic pressure only) Case II penetration model does not include any appreciable molecular weight effects. The molar volume ratio X only influences osmotic pressure [eq. (20)] at very low MW. Even if differential swelling stress were considered, accounting for this term [eq. (19)] would favor higher rates at higher MW, since this contribution to the overall stress relaxes more slowly at higher MW. We originally envisioned that the dependence of dissolution rate on MW could be explained by the variation of the effective surface concentration with MW. The slight slope in the penetration rate curve (Fig. 10) is due to the change in surface concentration with polymer MW. Clearly, the molecular weight dependence given by the energetics of a swollen network is not sufficient to account for the experimental observations. While the energetics of network entanglements provides a way to estimate the surface concentration during dissolution, which in itself is very useful, it does not explain the MW-dependent dissolution rates seen with PMMA in ketones.

Thus, MW effects must be included in the Case II model by allowing one or more of the parameters, K, a, or σ_c in eqs. (18) and (19) to be functions of MW. There is no physical basis for expecting the parameter a to depend on the polymer MW. The parameter K is similar to a creep compliance, and for temperatures below T_g, it is expected to be independent of MW.[38] However, it is reasonable to expect that σ_c should be a function of MW since it can be argued that longer chains can support higher stress levels before the onset of

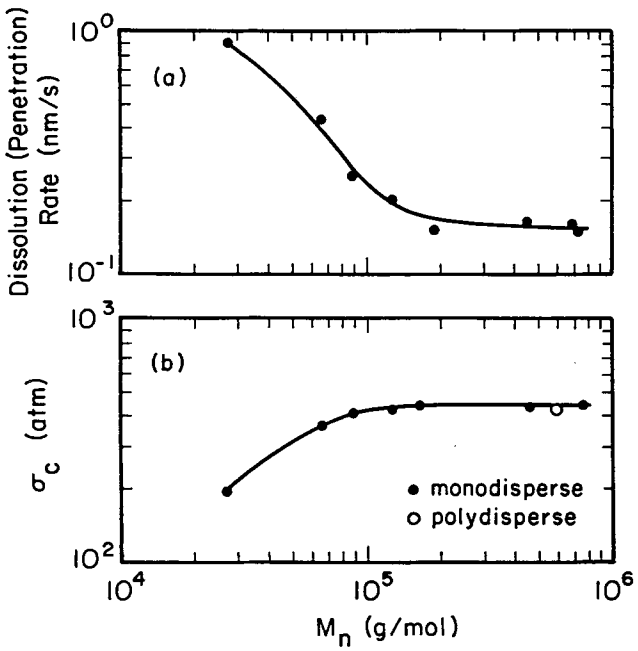

Fig. 11. (a) Dissolution data from Fig. 10 and Case II penetration rate curve based on a critical stress that varies with the polymer MW. (b) Calculated σ_c values versus number average molecular weight using experimental dissolution rates and the same values of a and K as in Fig. 10. These values of σ_c were used to generate the curve in part (a).

crazing. While this contention is supported in the literature,[39] mechanical crazing data for PMMA[33] suggest that σ_c is relatively insensitive to MW for the MW range 1.2×10^5–2.2×10^6 g/mol. The lower end of this range is approximately where the dissolution rate is seen to level off. Thus, it is possible that σ_c increases with MW at lower MW (thus decreasing the penetration rate), and then levels off.

Figure 11(a) shows a penetration rate curve based on a σ_c that varies with polymer MW. Clearly, a good fit of the dissolution data is possible when σ_c is adjusted for MW. Values of σ_c vs. MW are shown in Figure 11(b). These σ_c values were calculated from the experimental data with the same values of K, π, and a used to generate the penetration rate curve in Figure 10. Also shown in Figure 11(b) is the value of σ_c (polydisperse) upon which the predicted curve in Figure 10 is based. The leveling off of σ_c at approximately 1×10^5 g/mol is similar to that seen for the surface fracture energy of PMMA.[40] Since crazing is a precursor to fracture, the underlying physics should be similar. However, while the trend in σ_c is comparable to that for the surface fracture energy, the surface fracture energy changes by several orders of magnitude compared to a factor of 2–3 for σ_c over a similar MW range.[40] Further investigation of the dependence of penetration rate on polymer MW is needed.

The close connection between crazing and cracking raises one final issue for discussion. It is conceivable that, at low MW, PMMA cannot support the

osmotic stress induced by MIBK, and cracks develop at the surface of the film. Solvent could then penetrate along the cracks, resulting in enhanced dissolution rates. Stress cracking has been reported for PMMA (MW = 1.1×10^5 g/mol) dissolving in dimethylphthalate.[41] Furthermore, the MW where σ_c levels off is only about four times the critical molecular weight of PMMA ($M_c = 2.7 \times 10^4$ g/mol).[26] At molecular weights much below 1×10^5 g/mol, the degree of entanglement might be inadequate to suppress cracking. It must be emphasized, however, that even if low MW films do indeed crack, the validity of the stress-driven penetration model is not reduced. On the contrary, the usefulness of this model becomes evident. Both crazing and cracking are stress-driven, and the formation of cracks (and the subsequent enhancement of penetration rate) can be accounted for readily with a critical stress that depends on the polymer MW.

CONCLUSIONS

Models were developed to describe the swelling and dissolution of thin polymer films in terms of solvent penetration and surface disentanglement of polymer chains. The models account for both Fickian and Case II diffusion mechanisms. Reptation theory was used to scale the disentanglement rate with polymer molecular weight and solvent concentration. ,The effective solvent concentration at the surface of a dissolving film is a critical parameter since it determines the penetration rate, at least initially, for Case II diffusion, as well as the disentanglement rate. Thermodynamics of swollen networks was used to estimate this effective concentration.

The models can be used to guide the selection of processing conditions for microlithography. The utility of the models for selecting solvents which give desirable dissolution rates was demonstrated. In order to minimize swelling, the resist dissolution rate should be controlled by solvent penetration, not disentanglement of the polymer chains. The models can be used to estimate the MW range where dissolution is penetration controlled.

Comparison of predicted dissolution rates with experimental data for PMMA dissolving in MIBK (penetration controlled) revealed that the Case II model underestimates the effects of polymer MW on solvent penetration rates for MW $< 1.5 \times 10^5$ g/mol. To obtain good agreement with experimental data, the critical stress for crazing was modified to be a function of polymer MW. The functional dependence of σ_c on MW as calculated from experimental dissolution rates is similar qualitatively to that for the surface fracture energy of PMMA. The dependence of penetration rate on MW at relatively low MW needs to be investigated further.

This work was supported by the Air Force Office of Scientific Research under Grant No. AFOSR-90-0078. IBM 3081 and IBM 3090 computer time was provided by a DACE grant from the IBM Corp.

APPENDIX: NOMENCLATURE

a constant to convert pressure to axial stress
A molecular weight exponent
B high molecular weight rate constant

C disentanglement rate constant
C_s solvent mass concentration
D solvent diffusivity
D_D diffusional Deborah number
D_0 solvent diffusivity front factor
D_s solvent diffusivity
E_a apparent activation energy
ΔG free energy; subscripts are total, mixing and elastic
j_s local solvent mass flux
j_s' diffusive velocity
k Boltzmann's constant
K penetration rate front factor
L initial thickness
M molecular weight
M_c critical molecular weight for the onset of entanglements
M_e molecular weight between entanglements
M_f fragmented molecular weight
M_n number average molecular weight
MW molecular weight
n_1 number of solvent molecules
n_2 number of polymer molecules
N Avogadro's number
N_e number of moles of entanglements
R dissolution rate or gas constant
R dimensionless dissolution velocity
R_{dis} disentanglement rate
R_g radius of gyration
R_0 dissolution rate constant
ΔS entropy change
t_D characteristic diffusion time
t_{rep} characteristic reptation time
t_R characteristic relaxation time
T absolute temperature
T_g glass transition temperature
v local swelling velocity
v_2 penetration velocity
V final volume of swollen polymer
V_0 initial volume of polymer
V_1 solvent molar volume, or volume of solvent in control volume
V_2 polymer molar volume, or volume of polymer in control volume
w_s mass fraction solvent
x spatial position
x_1 location of gel-solvent interface
x_2 location of gel-glass interface
X ratio of polymer molar volume to solvent molar volume = V_2/V_1

Greek

α molecular weight exponent, or extension ratio for swelling
β constant in diffusivity function
γ constant for critical stress level
η dimensionless spatial coordinate = x/L
η_1 dimensionless position of gel-solvent interface
η_2 dimensionless position of gel-glass interface
μ_1 chemical potential of the solvent in the polymer
μ_1^0 chemical potential of the pure solvent
π^E excess stress

π_{eq} equilibrium osmotic stress
ρ density of the mixture, or ratio of complex amplitudes
ρ_i density of component i
σ_e twice the number of effective cross-links
σ total stress
σ_c critical stress for crazing = $\gamma(T_g - T)$
σ_{ds} differential swelling stress
τ dimensionless time
ϕ volume fraction, solvent volume fraction
ϕ^* solvent volume fraction in the polymer at gel-solvent interface
χ Flory-Huggins interaction parameter

Subscripts

1 solvent, or gel–solvent interface
2 polymer, or gel–glass interface

References

1. J. S. Vrentas, C. M. Jarzebski, and J. L. Duda, *AIChE J.*, **21**, 894 (1975).
2. J. S. Vrentas and J. L. Duda, *AIChE J.*, **25**, 1 (1979).
3. T. A. Alfrey, E. F. Gurnee, and W. G. Lloyd, *J. Polym. Sci. (C)*, **12**, 249 (1966).
4. N. Thomas and A. H. Windle, *Polymer*, **19**, 255 (1978).
5. J. Crank and G. S. Park in *Diffusion in Polymers*, J. Crank and G. S. Park, Eds., Academic, London, 1968, pp. 1–39.
6. J. Crank, *The Mathematics of Diffusion*, 2nd ed., Clarendon, Oxford, 1975.
7. G. S. Hartley and J. Crank, *Trans. Faraday Soc.*, **45**, 801 (1949).
8. J. H. Petropoulos and P. P. Roussis, *J. Membr. Sci.*, **3**, 343 (1978).
9. J. Crank, *J. Polym. Sci.*, **11**, 151 (1953).
10. N. L. Thomas and A. H. Windle, *Polymer*, **23**, 529 (1982).
11. C. Gostoli and G. C. Sarti, *Polym. Eng. Sci.*, **22**, 1018 (1982).
12. G. C. Sarti, C. Gostoli, G. Riccioli, and R. G. Carbonell, *J. Appl. Polym. Sci.*, **32**, 3627 (1986).
13. F. Asmussen and K. Ueberreiter, *J. Polym. Sci.*, **57**, 199 (1962).
14. J. S. Greeneich, *J. Electrochem. Soc.*, **122**, 970 (1975).
15. Y. Tu and A. C. Ouano, *IBM J. Res. Develop.*, **21**, 131 (1977).
16. F. H. Dill, W. P. Hornberger, P. S. Hauge, and J. M. Shaw, *IEEE Trans. Electron Devices*, **ED-22**, 445 (1975).
17. D. J. Kim, W. G. Oldham, and A. R. Neureuther, *IEEE Trans. Electron Devices*, **ED-31**, 1730 (1984).
18. M. P. C. Watts, *J. Vac. Sci. Technol.*, **B3**, 434 (1985).
19. C. A. Mack, *J. Electrochem Soc.*, **134**, 148 (1987).
20. J. S. Papanu, D. W. Hess, D. S. Soane (Soong), and A. T. Bell, *J. Appl. Polym. Sci.*, to appear.
21. J. S. Papanu, D. W. Hess, D. S. Soane (Soong), and A. T. Bell, *J. Electrochem. Soc.*, **136**, 1195 (1989).
22. P. J. Flory, *Principles of Polymer Chemistry*, Cornell University Press, Ithaca, NY, 1953, p. 495.
23. P. G. de Gennes and L. Leger, *Ann. Rev. Phys. Chem.*, **33**, 49 (1982).
24. P. G. de Gennes, *Scaling Concepts in Polymer Physics*, Cornell University Press, Ithaca, NY, 1979, p. 219.
25. P. J. Flory, *Principles of Polymer Chemistry*, Cornell University Press, Ithaca, NY, 1953, p. 576.
26. W. W. Graessley, *Adv. Polym. Sci.*, **16**, 1 (1974).
27. J. Crank, *Free and Moving Boundary Problems*, Clarendon, Oxford, 1984.
28. J. Crank, *Quart. J. Mech. Appl. Math., Part 2*, **10**, 220 (1957).
29. J. S. Papanu, Ph.D. dissertation, University of California, Berkeley, 1988.
30. D. W. Van Krevelen, *Properties of Polymers*, Elsevier, Amsterdam, 1976, p. 416.

31. H. Fujita, A. Kishimoto, and K. Matsumoto, *Trans. Faraday Soc.*, **56**, 424 (1960).
32. A. C. Ouano, *Polym. Eng. Sci.*, **18**, 306 (1978).
33. W. Doll, in *Crazing in Polymers*, H. H. Kausch, Ed., Adv. Polym. Sci., **52/53**, 1983, p. 105.
34. C. J. Sheehnan and A. L. Bisio, *Rubber Chem. Technol.*, **39**, 149 (1966).
35. J. Manjkow, J. S. Papanu, D. W. Hess, D. S. Soong, and A. T. Bell, *J. Electrochem. Soc.*, **134**, 2003 (1987).
36. W. J. Cooper, P. D. Krasicky, and F. Rodriguez, *Polymer*, **26**, 1071 (1985).
37. S. S. Sternstein, L. Ongchin, and A. Silverman, *Appl. Polym. Symp.*, **7**, 175 (1968).
38. L. E. Nielsen, *Mechanical Properties of Polymers and Composites*, Dekker, New York, 1974, Vol. I, p. 52.
39. L. E. Nielsen, *Mechanical Properties of Polymers and Composites*, Dekker, New York, 1974, Vol. I, p. 96.
40. R. P. Kusy and D. T. Turner, *Polymer*, **17**, 164 (1976).
41. K. Ueberreiter, in *Diffusion in Polymers*, J. Crank and G. S. Park, Eds., Academic, New York, 1968, p. 220.

Received January 20, 1988
Accepted August 18, 1988